THE JOURNAL OF PHYSICAL CHEMISTRY LETTERS
A JOURNAL OF THE AMERICAN CHEMICAL SOCIETY

pubs.acs.org/JPCL

Letter

Atomic Layer Deposition-Assisted Surface-Selective Isotopic Labeling for the ^{17}O Solid-State NMR Studies of Metal Oxide Surfaces

Junchao Chen, Xiao Liu, Li Shen,* Kuizhi Chen, Yujie Wen, Yang Wang, Xiaoli Xia, Fang Wang, Jennifer S. Gomez, Ivan Hung, Weiping Tang, Zhehong Gan, Jia-Huan Du,* Rong Chen,* and Luming Peng*

Cite This: *J. Phys. Chem. Lett.* 2025, 16, 6907−6913

Read Online

ACCESS | Metrics & More | Article Recommendations | Supporting Information

ABSTRACT: ^{17}O solid-state NMR spectroscopy is widely used to investigate metal oxide surfaces and is increasingly recognized for the unique insights into surface structures. Given the low natural abundance of the ^{17}O nucleus (0.037%), ^{17}O surface-selective isotopic labeling is commonly employed in relevant studies. Conventional thermal treatment (CTT)-labeling methods rely on rapid $^{17}O/^{16}O$ exchange may yield insufficient labeling on less reactive surfaces. Our approach uses atomic layer deposition (ALD) epitaxial growth to directly deposit ^{17}O onto metal oxide surfaces regardless of surface reactivity. This method minimizes the formation of excessive surface hydroxyl groups, reducing overlapping NMR signals and enabling better ^{17}O NMR identification of hydroxyl groups, as observed in Al_2O_3. Moreover, heteronuclear $^{27}Al\{^{17}O\}$ *J*-HMQC NMR analysis reveals that the CTT method creates more correlations between penta-coordinated Al sites and hydroxyl groups in Al_2O_3 compared to ALD, indicating that the labeling techniques vary in their effectiveness at different surface sites.

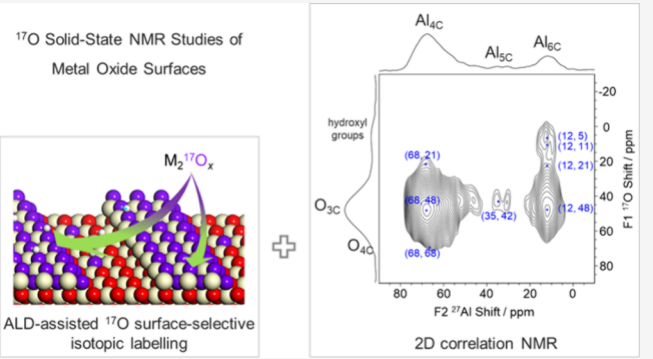

Surface oxygen ions in metal oxides play a crucial role across various fields, including heterogeneous catalysis,[1] chemical sensing,[2] environmental remediation,[3] solar fuel photocatalysis,[4] and battery technologies.[5] Therefore, deciphering these surface structures at the atomic scale to establish correlations with observed properties has been a focal point of research for many years.[6−8] In contrast to traditional surface determination methods that rely on high vacuum, such as microscopy,[9] which only probe a limited area of a particle and lack volume-averaging capabilities, ^{17}O solid-state nuclear magnetic resonance (ssNMR) has emerged as a complementary technique that is capable of providing site-specific insights representing the entire sample, even under atmospheric pressure conditions.[6,10,11] However, the extremely low natural abundance of the only NMR-active stable oxygen isotope, ^{17}O, presents a significant challenge to its widespread usage in many scenarios.[12,13] Over the past 3 decades, significant advancements have been made in developing isotopic labeling strategies to increase the concentration of the ^{17}O nucleus in the target samples under investigation.[6,12] These strategies include ionothermal synthesis using ^{17}O-enriched water ($H_2{}^{17}O$),[14] high-temperature thermal treatment with ^{17}O-enriched oxygen gas ($^{17}O_2$) at temperatures of 673 K or higher,[15] and mechano-synthesis using $H_2{}^{17}O$ in a ball-milling apparatus.[16] Nevertheless, these methods predominantly label the bulk, leading to limited selectivity for the surfaces, which is crucial for applications in adsorption and catalysis. In 2015, Wang and co-workers[17] demonstrated a surface-selective enrichment approach using ceria nanomaterials as an illustrative example, with $H_2{}^{17}O$ coupled with thermal treatment at relatively low temperatures (less than 373 K). Since then, the combined approach of this labeling method with ^{17}O solid-state NMR spectroscopy and density functional theory calculations to investigate the detailed surface structure of metal oxides and related gas adsorption/activation has become increasingly popular.[18−27] However, this conventional thermal treatment (CTT)-labeling method highly relies on surface reactivity,[6] which limits its broader applicability. Therefore, there is a pressing need to develop alternative ^{17}O surface-selective labeling approaches.

Received: April 14, 2025
Revised: June 22, 2025
Accepted: June 24, 2025
Published: June 28, 2025

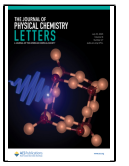

https://doi.org/10.1021/acs.jpclett.5c01138
J. Phys. Chem. Lett. 2025, 16, 6907−6913

Atomic layer deposition (ALD) is a technique for controlled surface fabrication characterized by its atomic-level growth control. It involves exposing a substrate to alternating chemical vapors, allowing reactions to occur in a self-limiting and sequential manner.[28−31] This technology is notable for its precise thickness control and excellent uniformity across surfaces.[28] Specifically, ALD utilizes highly reactive metal−organic compound precursors that react with water to enable the epitaxial growth of many oxides, such as MgO,[32] ZnO,[33] and Al_2O_3.[34] In this study, we developed a method for efficient ^{17}O surface-selective labeling using ALD. This technique involves a single reaction cycle where metal−organic compounds react with $H_2{}^{17}O$, ensuring that the majority of ^{17}O is incorporated into the surfaces rather than the bulk. By conducting high-field and two-dimensional correlation ^{17}O NMR measurements, we were able to detail the surface structures of Al_2O_3 under different labeling schemes. This study introduces an alternative ^{17}O surface-selective labeling approach to reveal the surface structures of metal oxides. Extending this ALD-based ^{17}O-labeling approach to investigate the detailed surface structures of other metal oxides can be readily envisaged. Many metal oxide surfaces, such as TiO_2, MgO, ZrO_2, HfO_2, ZnO_2, Ta_2O_5, Nb_2O_5, and V_2O_5,[32−34] can be deposited by ALD using H_2O as the oxygen source. Additionally, it highlights the importance of selecting appropriate labeling schemes for tailoring different surface sites.

In a typical ^{17}O-labeling procedure using ALD, an organometallic precursor [such as $Mg(CpEt)_2$,[32] $Zn(CH_2CH_3)_2$,[33] $Al(CH_3)_3$,[28,34] etc.] reacts with the original hydroxyl groups on the surface of the metal oxide particles, all within a controlled temperature and vacuum chamber. The ALD process comprises three steps (Figure 1): (1) A short

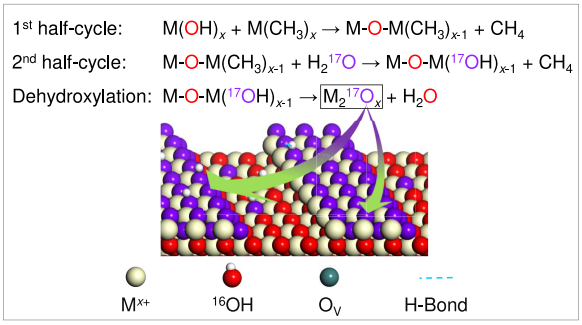

Figure 1. Schematic of the ALD-assisted ^{17}O surface-selective isotopic labeling scheme. "M" refers to the complexed metal cation.

pulse of the organometallic precursor reacts with the substrate's hydroxyl groups, forming $M-O-M(CH_3)_{x-1}$ species (where M represents the metal element and x is its valence state) and the byproduct of gaseous CH_4. (2) A purge of $H_2{}^{17}O$ converts $M-O-M(CH_3)_{x-1}$ into ^{17}O-labeled $M-O-M(OH)_{x-1}$ [abbreviated by $M-O-M(^{17}OH)_{x-1}$] and continues to release the byproduct of gaseous CH_4. (3) The $M-O-M(^{17}OH)_{x-1}$ species are usually converted into ^{17}O-labeled $M_2{}^{17}O_x$ layers through dehydroxylation processes at elevated temperatures. Unlike traditional ALD processes in which multiple cycles are used to form a relatively "thick" layer, this ALD-based labeling method completes in a single cycle, depositing one layer onto the surface of metal oxides. In contrast to the CTT approach (Figure S1), which relies on the rapid exchange of lattice oxygen (^{16}O) with adsorbed $H_2{}^{17}O$, the ALD method employs highly reactive organometallic precursors that directly incorporate ^{17}O anions into the surface lattice and, therefore, does not depend on surface reactivity.

To demonstrate the feasibility of the proposed ALD-based ^{17}O surface-selective labeling scheme, Al_2O_3, a metal oxide crucial for heterogeneous catalysis,[35−37] is employed as a model to illustrate this approach. Its surface hydroxyl groups and aluminum cations serve as Brønsted and Lewis acidic sites, respectively, which are essential in facilitating many hydration and dehydration reactions.[28] Al_2O_3 nanoparticles were prepared by annealing boehmite colloidal powders and were then subjected to ^{17}O labeling with ALD (one cycle; see methods) and CTT methods, respectively. The resulting samples were named ALD-Al_2O_3 and CTT-Al_2O_3 according to the labeling scheme. The powder X-ray diffraction (XRD) patterns depicted in Figure S2 reveal minimal distinctions and can be collectively indexed as Al_2O_3. This observation suggests that the labeling processes did not alter the bulk structure. High-resolution transmission electron microscopy (HRTEM) images (Figure S3) reveal that these labeled nanoparticles present dimensions ranging from approximately 2 to 6 nm in width. The Brunauer−Emmett−Teller (BET) surface areas of ALD-Al_2O_3 and CTT-Al_2O_3 (Figure S4a and Table S1) are measured as 172.4 and 195.4 $m^2\ g^{-1}$, respectively, while their average pore sizes remain consistent at around 5.5 nm (Figure S4b). Potential impurities containing carbon or nitrogen originating from the boehmite colloidal precursor or the surrounding environment are not discernible through $^{13}C\{^1H\}$ cross-polarization (CP) magic angle spinning (MAS) NMR, as illustrated in Figure S5, nor through elemental analysis, as indicated in Table S1. Thus, surface impurities can be disregarded in a subsequent investigation.

^{17}O MAS NMR measurements on ALD-Al_2O_3 (Figure 2a) and CTT-Al_2O_3 (Figure 2b) were then conducted at two field strengths of 19.6 and 9.4 T, respectively. Because the NMR shift and line width of a quadrupolar nucleus (spin number $I > 1/2$, such as ^{17}O and ^{27}Al) depend on the strength of the applied magnetic field (i.e., a higher field gives rise to a resonance with the center of gravity at a higher frequency and a narrower line width),[38] the ^{17}O NMR signals exhibit noticeable shifts and a reduction in overall line broadening at 19.6 T compared to those observed at 9.4 T. The moderately broad ^{17}O signals at 11 ppm for ALD-Al_2O_3 and 10 ppm for CTT-Al_2O_3 at 19.6 T, respectively, shifting to −45 and −23 ppm at 9.4 T, can be attributed to hydroxyl groups on the surfaces of Al_2O_3 according to previous studies;[39] the peak at 48 ppm at 19.6 T, which shifts to 40 ppm at 9.4 T in both samples, can be ascribed to the surface tri-coordinated oxygen anions (O_{3C}s);[39] and the shoulder peak at 68 ppm, which remains unaffected by both the field strength and labeling method, can be assigned to the surface tetra-coordinated oxygen anions (O_{4C}s).[39] Notable differences in NMR shifts are observed for the hydroxyl groups and O_{3C}s at different magnetic fields, stemming from substantial quadrupolar interactions. Conversely, the similarity in the frequencies of the signals due to the presence of O_{4C}s at 19.6 and 9.4 T is associated with their very small quadrupolar interaction. In contrast to the prominent ^{17}O signals observed in CTT-Al_2O_3 (10 ppm at 19.6 T and −23 ppm at 9.4 T), which originate from surface hydroxyl species, the intensities of these signals in ALD-Al_2O_3 (11 ppm at 19.6 T and −45 ppm at 9.4 T) are relatively low, suggesting that the ALD-labeling approach introduces fewer hydroxyl groups. Using the same

https://doi.org/10.1021/acs.jpclett.5c01138
J. Phys. Chem. Lett. 2025, 16, 6907−6913

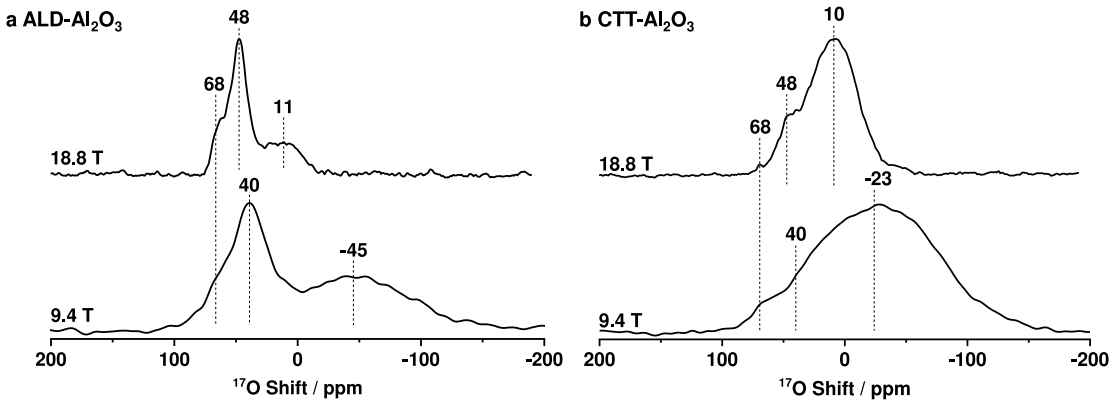

Figure 2. ^{17}O MAS NMR spectra of ^{17}O-labeled ALD-Al_2O_3 and CTT-Al_2O_3 recorded at 9.4 and 19.6 T, respectively. The experimental durations were 6.8 min at 19.6 T and 11.1 h at 9.4 T for ALD-Al_2O_3, and 6.8 min at 19.6 T and 2.8 h at 9.4 T for CTT-Al_2O_3.

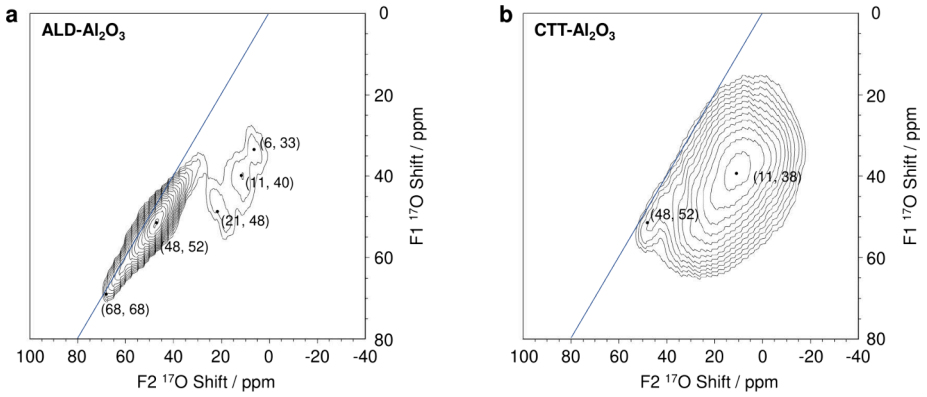

Figure 3. ^{17}O MQMAS spectra of ^{17}O-labeled ALD-Al_2O_3 and CTT-Al_2O_3. External field, 19.6 T; MAS rate, 16 kHz; and recycle delay, 0.5 s. The experiment takes 16.7 h for ALD-Al_2O_3 compared to 12.8 h for CTT-Al_2O_3.

batch of the unenriched γ-Al_2O_3 substrate, we prepared a second ALD-Al_2O_3 sample under identical ALD conditions. Figure S6 compares its ^{17}O NMR spectrum (recorded at 19.6 T) with that shown in Figure 2a. The similar shifts, signal to noise, and line widths in both spectra demonstrate that our ALD-labeling scheme is reproducible.

Nevertheless, despite employing ALD labeling and high-field recording (19.6 T), the resolution of 1D ^{17}O NMR remains insufficient for distinguishing distinct hydroxyl species. This limitation is likely due to the broadening caused by wide chemical shift distributions resulting from hydrogen bonds and moderately large quadrupolar interactions. We subsequently conducted 2D multiple quantum MAS (MQMAS)[37] NMR experiments, which are powerful for removing second-order quadrupolar line broadening (Figure 3 and Figure S7). According to the observed shifts at F2 and F1 dimensions [illustrated by (δ_{F2}, δ_{F1}), where δ_{F2} is equivalent to the center of gravity (δ_{CG}) shown in the 1D spectra in Figure 2], NMR parameters, including quadrupole-induced shift (δ_{QIS}), quadrupolar interaction product (P_Q), and isotropic chemical shift (δ_{iso}), can be extracted (Table S2). δ_{QIS} and P_Q are related to quadrupolar interactions, which are magnetic-field-dependent, while δ_{iso} is unaffected by the external magnetic field.[40,41] These NMR parameters follow the relationships outlined below[41]

$$\delta_{F1} = \delta_{iso} - (10/17) \times \delta_{QIS}$$

$$\delta_{F2} = \delta_{iso} + \delta_{QIS}$$

$$\delta_{QIS} = -6000 \times (P_Q/\nu_L)^2$$

where ν_L is the Larmor frequency of the ^{17}O nucleus at 19.6 T (112.7 MHz). The peak at (68, 68) ppm in the spectrum of ALD-Al_2O_3 (Figure 3a), which represents surface O_{4C} sites, exhibits identical values for both δ_{F2} and δ_{F1}. This indicates the very small quadrupolar interaction associated with this site, consistent with the data in Figure 2. This signal is very small in the spectrum for CTT-Al_2O_3 in Figure 3b, likely due to the optimized MQMAS parameters focusing primarily on enhancing strong signals, leaving weaker ones less pronounced. The resonance at (48, 52) ppm, attributed to the surface O_{3C} site, is observed in both samples. The difference of 4 ppm corresponds to a δ_{QIS} of −2.5 ppm at 19.6 T and a P_Q of 2.3 MHz. Hence, the quadrupolar interaction of the O_{3C} sites is more pronounced compared to that of the O_{4C} sites. The broad peak centered at 11 ppm in the 1D data of ALD-Al_2O_3 (top line in Figure 2a) splits into three distinct resonances in the 2D MQMAS spectrum (Figure 3a). These resonances, positioned at (21, 48), (11, 40), and (6, 33) ppm, are attributed to the triply bridging (μ_3-OH), doubly bridging (μ_2-OH), and singly terminal (μ_1-OH) hydroxyl groups, respectively.[42,43] The slices corresponding to the three resonances in Figure 3a were extracted along the F2 dimension and fitted (Figure S8). The various NMR parameters extracted [δ_{iso}, quadrupole coupling constants (C_Q), and asymmetry parameters (η)] indicate distinct local environments for the associated hydroxyl species. For CTT-Al_2O_3, these sites continue to overlap, and a broad peak at (11, 38) ppm can

https://doi.org/10.1021/acs.jpclett.5c01138
J. Phys. Chem. Lett. 2025, 16, 6907−6913

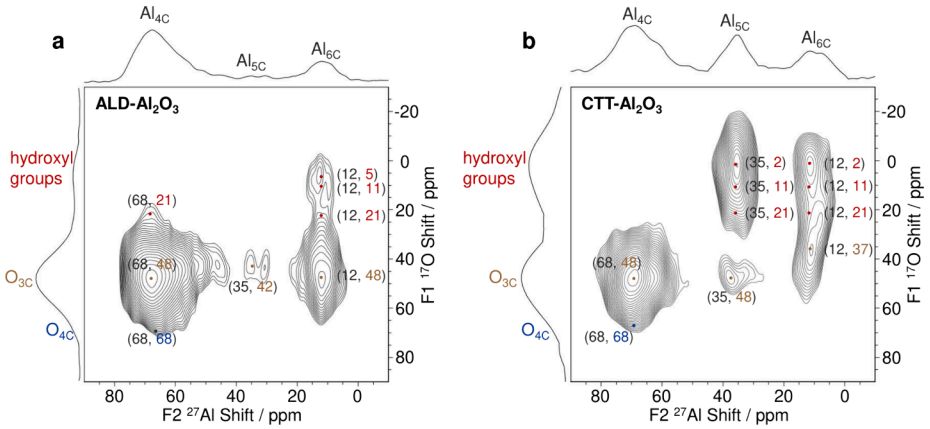

Figure 4. 2D ^{27}Al{^{17}O} *J*-HMQC correlation spectra of ^{17}O-labeled ALD-Al_2O_3 and CTT-Al_2O_3. External field, 18.8 T; MAS rate, 16 kHz; and recycle delay, 0.1 s. The experiment takes 10.3 h for ALD-Al_2O_3 compared to 7.9 h for CTT-Al_2O_3.

be observed in the 2D MQMAS spectrum (Figure 3b), despite the removal of second-order quadrupole broadening. This disparity highlights that the broadening of the ^{17}O NMR peaks in CTT-Al_2O_3, corresponding to hydroxyl species, results from both chemical shift distribution and quadrupole interaction, whereas the broadening observed in ALD-Al_2O_3 primarily results from quadrupolar interactions. In comparison to the ^{17}O signals from O_{3C} and O_{4C} sites, the signals from hydroxyl sites show larger differences in δ_{iso} and δ_{F2}, owing to larger P_Q values (2.3 or 0 MHz for O_{3C} and O_{4C} sites vs around 6 MHz for hydroxyl sites) (Table S2). The stronger quadrupolar interactions of these hydroxyl groups than the surface lattice can be attributed to their binding with highly electronegative hydrogen atoms.[44]

^{27}Al NMR spectra are then recorded to complement the observations in ^{17}O NMR. The ^{27}Al signals resonating at 12, 35, and 68 ppm are respectively attributed to the hexa-, penta-, and tetra-coordinated Al sites (Al_{4C}, Al_{5C}, and Al_{6C} sites)[35,39] (Figure S9). Because most Al_{4C} and Al_{6C} sites originate from the bulk, while only Al_{5C} sites are surface-derived,[45] the similarities in shifts, intensities, and line widths observed for both ALD-Al_2O_3 and CTT-Al_2O_3 suggest that the ALD-labeling scheme does not affect the amount of surface Al_{5C} sites.

Furthermore, the Al surface sites of Al_2O_3 can be selectively observed through 2D correlation NMR techniques with ^{17}O surface-selective isotopic labeling. The 2D ^{17}O{^{27}Al} *J*-heteronuclear multiple quantum coherence (HMQC) spectra[46] showcase chemical bond correlations of surface ^{17}O to ^{27}Al facilitated by scalar-coupling transfer (Figure 4). Based on above-mentioned observations, the bare O_{4C}s, O_{3C}s, as well as oxygen in μ_3-OH, μ_2-OH, and μ_1-OH respectively resonate at approximately 68, 48 (42/37), 21, 11, and 5 (2) ppm in the F1 dimension of panels a and b of Figure 4. Meanwhile, the aluminum peaks appearing at 68, 35, and 12 ppm in the F2 dimension are owing to the Al_{4C}, Al_{5C}, and Al_{6C} sites, respectively. Under both labeling schemes, bare O_{3C} exhibits a strong correlation signal with all aluminum sites (Al_{4C}, Al_{5C}, and Al_{6C}), while bare O_{4C} displays only a connection with Al_{4C}. Considering that CTT-Al_2O_3 exhibits stronger ^{17}O NMR resonance of surface hydroxyl groups compared to ALD-Al_2O_3, different findings emerge when linking Al sites with O from hydroxyl groups: (1) Strong Al_{6C}–(μ_3-OH), Al_{6C}–(μ_2-OH), and Al_{6C}–(μ_1-OH) correlations are present in both spectra, suggesting that a significant number of surface hydroxyl groups can coordinate with Al_{6C} sites in the triply, doubly, and singly bonded forms; (2) In both samples, NMR correlations for Al_{4C}–O_{4C}, Al_{4C}–O_{3C}, Al_{5C}–O_{3C}, and Al_{6C}–O_{3C} are observed, while correlations for Al_{5C}–O_{4C} and Al_{6C}–O_{4C} are absent. This indicates that labeling of these surface non-hydroxyl sites is independent of the labeling methods used and that not all Al environments can bond with surface O_{4C} sites; (3) ALD-Al_2O_3 exhibits the Al_{4C}–(μ_3-OH) correlation, which is absent for CTT-Al_2O_3; conversely, a strong Al_{5C}–OH signal can be observed for CTT-Al_2O_3 but not for ALD-Al_2O_3. These results agree well with the mechanism for ^{17}O exchange on γ-Al_2O_3 surfaces, in which H_2O is activated at Al_{4C} sites to form two OH groups and generate a new Al_{5C} site.[47−49] The contrast highlights the varying effectiveness of different labeling methods in enriching various surface hydroxyl groups, which may result from differences in labeling mechanisms, i.e., ^{17}O surface deposition for the ALD scheme and ^{17}O/^{16}O exchange for the CTT scheme. This emphasizes that selecting appropriate ^{17}O isotopic labeling schemes is essential for ^{17}O NMR studies of the Al_2O_3 surfaces. To differentiate specific surface hydroxyl groups, which are the Brønsted acid centers and are crucial for surface acidity/basicity modulations,[36,37] the ALD-based scheme may be more feasible. In contrast, when surface coordination-unsaturated Al_{5C} sites that serve as Lewis acid centers or anchoring sites for supported species are studied,[35,50] the CTT method can be preferable. By comparing the similar ^{27}Al NMR spectra of ALD-Al_2O_3 and CTT-Al_2O_3 (Figure S9) and considering the FTIR data from the literature that point to a similar OH formation mechanism,[47−49] we conclude that the ALD-grown sample is likely to resemble the original γ-Al_2O_3. Therefore, we believe that neither the Lewis nor Brønsted acid sites have undergone significant change.

We developed an ALD-based surface-selective ^{17}O isotopic labeling method specific to investigate metal oxide surfaces. In comparison to the CTT scheme, which relies on surface reactivity, the ALD-based method incorporates ^{17}O anions directly into the surface lattice, making it independent of surface reactivity. As demonstrated with Al_2O_3, the ALD scheme enables better NMR identification of surface hydroxyl groups compared to the CTT approach. In contrast, the CTT approach excels in labeling the oxygen sites connecting to coordination-unsaturated penta-coordinated Al_{5C} sites, the primary anchoring centers for supported species, and thus provides more detailed insights into the Al_{5C}–hydroxyl group correlations compared to the ALD scheme. These results

https://doi.org/10.1021/acs.jpclett.5c01138
J. Phys. Chem. Lett. 2025, 16, 6907−6913

demonstrate that the choice of isotopic labeling method significantly influences the characterization of metal oxide surfaces, and selecting a proper labeling method tailored to the specific surface site is essential for effective investigations.

Experimental Section. *Preparation of γ-Al_2O_3 Nanoparticles.* γ-Al_2O_3 nanoparticles were synthesized via annealing boehmite colloidal powders (Zhejiang Yuda Chemical Co., Ltd., China) at 823 K overnight.

^{17}O Isotopic Labeling: ALD Scheme. Al_2O_3 deposition was carried out using a home-built fluidized bed ALD reactor (AngstromBlock Scale-F015 ALD system). The ALD process was conducted at 473 K under a constant pressure of 160 Pa and divided into two half-cycles. Before deposition, the Al_2O_3 substrate was annealed at 473 K to eliminate surface-adsorbed impurities, followed by purging $H_2{}^{16}O$ vapor for 200 s to pre-hydroxylate the Al_2O_3 substrate surfaces for enhancing reactivity. In the first half-cycle, a 200 s pulse of $Al(CH_3)_3$ was applied to facilitate the reaction with the hydroxyl groups on the Al_2O_3 surfaces, leading to the formation of Al−O−$Al(CH_3)_2$ species on the surfaces of Al_2O_3. In the second half-cycle, a 200 s pulse of 90% ^{17}O-enriched $H_2{}^{17}O$ (∼2.1 mmol) was introduced to convert the Al−O−$Al(CH_3)_2$ species into ^{17}O-labeled Al−O−$Al(OH)_2$. Subsequently, the obtained samples were treated at 473 K to convert the Al−O−$Al(OH)_2$ species into surface ^{17}O-labeled Al_2O_3. Simultaneously, they were purged with N_2 for 30 min to eliminate any generated CH_4 gases before being transferred to a N_2-filled glovebox for further handling.

CTT Scheme. A 100 mg sample was subjected to evacuation at 473 K for 3 h within a quartz tube connected to a vacuum line for activation. Following cooling to 300 K, the tube was infused with 90% ^{17}O-enriched H_2O vapor (∼0.4 mmol) and maintained at room temperature for 20 h to achieve $H_2{}^{17}O$ enrichment. Finally, the sample was re-evacuated at room temperature to eliminate any residual $H_2{}^{17}O$ isotope.

Characterization of the ^{17}O Labeled γ-Al_2O_3 Nanopowders. The XRD measurements were carried out on a Shimadzu XRD-6000 diffractometer using Cu Kα radiation (λ = 1.54 Å) at 40 kV and 40 mA. HRTEM patterns were recorded on a JEOL JEM-2100 instrument with an accelerating voltage of 200 kV. BET specific surface area data were collected with nitrogen adsorption at 77 K on a Micromeritics Tristar 3020 apparatus. Pore size distribution information was calculated from the desorption data through the Barrett−Joyner−Halenda (BJH) method.

^{17}O Solid-State NMR Spectroscopy. ^{17}O single-pulse and MQMAS data were recorded at a Larmor frequency of 112.7 MHz using a 3.2 mm MAS probe on a Bruker NEO spectrometer operating at 19.6 T. A pulse width of 1.9 μs, equivalent to a solution state π/6 flip angle, was applied. High-field ^{27}Al single-pulse and 2D $^{27}Al\{^{17}O\}$ *J*-HMQC correlation NMR spectra were obtained at Larmor frequencies of 208.5 MHz (^{27}Al) and 108.4 MHz (^{17}O), respectively, on a Bruker Avance III spectrometer operating at 18.8 T and equipped with a 3.2 mm MAS probe. The pulse widths of 4.0 and 1.5 μs, which correspond to the solution state π/6 flip angles of ^{27}Al and ^{17}O nuclei, respectively, were used. Relatively low-field ^{17}O MAS NMR measurements were conducted at 54.2 MHz with a Bruker Avance III 400 spectrometer at 9.4 T utilizing a 3.2 MAS probe. The excitation pulse with a width of 0.4 μs, corresponding to a solution π/6 flip angle, was utilized for single-pulse experiments. ^{17}O and ^{27}Al chemical shifts were respectively referenced to distilled H_2O and 0.1 M $Al(NO_3)_3$ at 0.0 ppm. All of the ^{17}O-labeled samples were packed in a N_2-filled glovebox.

■ ASSOCIATED CONTENT

Supporting Information

The Supporting Information is available free of charge at https://pubs.acs.org/doi/10.1021/acs.jpclett.5c01138.

Characterization data and experimental NMR spectra (PDF)

■ AUTHOR INFORMATION

Corresponding Authors

Li Shen − *Key Laboratory of Mesoscopic Chemistry of MOE and Collaborative Innovation Center of Chemistry for Life Sciences, School of Chemistry and Chemical Engineering, Nanjing University, Nanjing 210023, China; Guangling College, Yangzhou University, Yangzhou 225009, China*; Email: shenli710@126.com

Jia-Huan Du − *State Key Laboratory of Materials-Oriented Chemical Engineering, College of Chemical Engineering, Nanjing Tech University, Nanjing 211816, China*; orcid.org/0000-0003-2408-0060; Email: dujiahuan12@126.com

Rong Chen − *State Key Laboratory of Digital Manufacturing Equipment and Technology, School of Mechanical Science and Engineering, School of Optical and Electronic Information, Huazhong University of Science and Technology, Wuhan 430074, China*; orcid.org/0000-0001-7371-1338; Email: rongchen@mail.hust.edu.cn

Luming Peng − *Key Laboratory of Mesoscopic Chemistry of MOE and Collaborative Innovation Center of Chemistry for Life Sciences, School of Chemistry and Chemical Engineering, Nanjing University, Nanjing 210023, China; Jiangsu Key Laboratory of Vehicle Emissions Control, Nanjing University, Nanjing 210093, China; Frontiers Science Center for Critical Earth Material Cycling (FSC-CEMaC), Nanjing University, Nanjing 210023, China*; orcid.org/0000-0003-1935-1620; Email: luming@nju.edu.cn

Authors

Junchao Chen − *School of Chemistry and Chemical Engineering, Shanghai Jiao Tong University, Shanghai 200240, China*; orcid.org/0000-0002-7601-5458

Xiao Liu − *State Key Laboratory of Digital Manufacturing Equipment and Technology, School of Mechanical Science and Engineering, School of Optical and Electronic Information, Huazhong University of Science and Technology, Wuhan 430074, China*; orcid.org/0000-0003-4178-5775

Kuizhi Chen − *State Key Laboratory of Catalysis, Dalian National Laboratory for Clean Energy, 2011-Collaborative Innovation Center of Chemistry for Energy Materials, Dalian Institute of Chemical Physics, Chinese Academy of Sciences, Dalian 116023, China*; orcid.org/0000-0002-9853-7070

Yujie Wen − *Key Laboratory of Mesoscopic Chemistry of MOE and Collaborative Innovation Center of Chemistry for Life Sciences, School of Chemistry and Chemical Engineering, Nanjing University, Nanjing 210023, China*

Yang Wang − *Key Laboratory of Mesoscopic Chemistry of MOE and Collaborative Innovation Center of Chemistry for Life Sciences, School of Chemistry and Chemical Engineering, Nanjing University, Nanjing 210023, China*

https://doi.org/10.1021/acs.jpclett.5c01138
J. Phys. Chem. Lett. 2025, 16, 6907−6913

Xiaoli Xia − *Key Laboratory of Mesoscopic Chemistry of MOE and Collaborative Innovation Center of Chemistry for Life Sciences, School of Chemistry and Chemical Engineering, Nanjing University, Nanjing 210023, China*
Fang Wang − *Key Laboratory of Mesoscopic Chemistry of MOE and Collaborative Innovation Center of Chemistry for Life Sciences, School of Chemistry and Chemical Engineering, Nanjing University, Nanjing 210023, China*
Jennifer S. Gomez − *Magnetic Resonance Research Center, Institute for Molecules and Materials, Radboud University, 6525 AJ Nijmegen, Netherlands*
Ivan Hung − *National High Magnetic Field Laboratory (NHMFL), Tallahassee, Florida 32310, United States;* orcid.org/0000-0001-8916-739X
Weiping Tang − *School of Chemistry and Chemical Engineering, Shanghai Jiao Tong University, Shanghai 200240, China*
Zhehong Gan − *National High Magnetic Field Laboratory (NHMFL), Tallahassee, Florida 32310, United States;* orcid.org/0000-0002-9855-5113

Complete contact information is available at: https://pubs.acs.org/10.1021/acs.jpclett.5c01138

Author Contributions

Junchao Chen, Li Shen, Jia-Huan Du, Rong Chen, and Luming Peng conceived the idea, designed the study, and coordinated the project. Junchao Chen, Jia-Huan Du, Li Shen, Kuizhi Chen, Ivan Hung, Zhehong Gan, and Luming Peng performed ^{17}O isotope enrichment by the conventional thermal treatment scheme and collected as well as analyzed the NMR spectra. Xiao Liu and Rong Chen conducted the ^{17}O isotope enrichment by the atomic layer deposition scheme. Yujie Wen, Yang Wang, Xiaoli Xia, and Fang Wang conducted other characterizations of the samples and analyzed the results. Weiping Tang and Jennifer S. Gomez provided valuable suggestions. Junchao Chen and Luming Peng wrote the manuscript. All authors discussed the experiments and final manuscript.

Notes

The authors declare no competing financial interest.

■ ACKNOWLEDGMENTS

This work was supported by the National Key R&D Program of China (2021YFA1502803), the National Natural Science Foundation of China (NSFC, 22472075, 22272075, 22402119, W2421041, 21972066, 92372103, and 91745202), and the NSFC−Royal Society Joint Program (21661130149). Luming Peng thanks the Royal Society and Newton Fund for a Royal Society−Newton Advanced Fellowship. This work was also supported by the research funds for the Frontiers Science Centre for Critical Earth Material Cycling, Nanjing University, and a project funded by the Priority Academic Program Development of Jiangsu Higher Education Institutions. Luming Peng and Junchao Chen thank Prof. Arno P. M. Kentgens and Dr. Ernst R. H. van Eck at Radboud University for their invaluable discussions and help in this work. A portion of this work was performed at the National High Magnetic Field Laboratory, which is supported by the National Science Foundation Cooperative Agreement DMR-1644779 and the State of Florida.

■ ABBREVIATIONS USED

CTT, conventional thermal treatment; ALD, atomic layer deposition

■ REFERENCES

(1) Védrine, J. C. Heterogeneous Catalysis on Metal Oxides. *Catalysts* **2017**, *7*, 341.
(2) *Metal Oxide Nanomaterials for Chemical Sensors*; Carpenter, M. A., Mathur, S., Kolmakov, A., Eds.; Springer: New York, 2013; DOI: 10.1007/978-1-4614-5395-6.
(3) Theerthagiri, J.; Chandrasekaran, S.; Salla, S.; Elakkiya, V.; Senthil, R. A.; Nithyadharseni, P.; Maiyalagan, T.; Micheal, K.; Ayeshamariam, A.; Arasu, M. V.; Al-Dhabi, N. A.; Kim, H.-S. Recent Developments of Metal Oxide Based Heterostructures for Photocatalytic Applications towards Environmental Remediation. *J. Solid State Chem.* **2018**, *267*, 35−52.
(4) Han, H.; Li, C. Photocatalysis in Solar Fuel Production. *Natl. Sci. Rev.* **2015**, *2*, 145−147.
(5) Tian, Y.; Zeng, G.; Rutt, A.; Shi, T.; Kim, H.; Wang, J.; Koettgen, J.; Sun, Y.; Ouyang, B.; Chen, T.; Lun, Z.; Rong, Z.; Persson, K.; Ceder, G. Promises and Challenges of Next-Generation "Beyond Li-ion" Batteries for Electric Vehicles and Grid Decarbonization. *Chem. Rev.* **2021**, *121*, 1623−1669.
(6) Chen, J.; Wang, F.; Wen, Y.; Tang, W.; Peng, L. Emerging Applications of ^{17}O Solid-State NMR Spectroscopy for Catalytic Oxides. *ACS Catal.* **2023**, *13*, 3485−3500.
(7) Anpo, M.; Costentin, G.; Giamello, E.; Lauron-Pernot, H.; Sojka, Z. Characterisation and Reactivity of Oxygen Species at the Surface of Metal Oxides. *J. Catal.* **2021**, *393*, 259−280.
(8) Rousseau, R.; Glezakou, V.-A.; Selloni, A. Theoretical Insights into the Surface Physics and Chemistry of Redox-Active Oxides. *Nat. Rev. Mater.* **2020**, *5*, 460−475.
(9) Hansen, T. W.; Wagner, J. B.; Hansen, P. L.; Dahl, S.; Topsøe, H.; Jacobsen, C. J. H. Atomic-Resolution in Situ Transmission Electron Microscopy of a Promoter of a Heterogeneous Catalyst. *Science* **2001**, *294*, 1508−1510.
(10) Shen, L.; Peng, L. ^{17}O Solid-State NMR Studies of Oxygen-Containing Catalysts. *Chin. J. Catal.* **2015**, *36*, 1494−1504.
(11) Bignami, G. P. M.; Dawson, D. M.; Seymour, V. R.; Wheatley, P. S.; Morris, R. E.; Ashbrook, S. E. Synthesis, Isotopic Enrichment, and Solid-State NMR Characterization of Zeolites Derived from the Assembly, Disassembly, Organization, Reassembly Process. *J. Am. Chem. Soc.* **2017**, *139*, 5140−5148.
(12) Xia, X.; Zhu, L.; Tang, W.; Peng, L.; Chen, J. A review of ^{17}O Isotopic Labeling Techniques for Solid-State NMR Structural Studies of Metal Oxides in Lithium-Ion Batteries. *Magn. Reson. Lett.* **2024**, *4*, No. 200120.
(13) Yang, L.; Huang, M.; Feng, N.; Wang, M.; Xu, J.; Jiang, Y.; Ma, D.; Deng, F. Unraveling the Atomic Structure and Dissociation of Interfacial Water on Anatase TiO_2 (101) under Ambient Conditions with Solid-State NMR Spectroscopy. *Chem. Sci.* **2024**, *15*, 11902−11911.
(14) Griffin, J. M.; Clark, L.; Seymour, V. R.; Aldous, D. W.; Dawson, D. M.; Iuga, D.; Morris, R. E.; Ashbrook, S. E. Ionothermal ^{17}O Enrichment of Oxides Using Microlitre Quantities of Labelled Water. *Chem. Sci.* **2012**, *3*, 2293−2300.
(15) Seymour, I. D.; Middlemiss, D. S.; Halat, D. M.; Trease, N. M.; Pell, A. J.; Grey, C. P. Characterizing Oxygen Local Environments in Paramagnetic Battery Materials via ^{17}O NMR and DFT Calculations. *J. Am. Chem. Soc.* **2016**, *138*, 9405−9408.
(16) Métro, T.-X.; Gervais, C.; Martinez, A.; Bonhomme, C.; Laurencin, D. Unleashing the Potential of ^{17}O NMR Spectroscopy Using Mechanochemistry. *Angew. Chem., Int. Ed.* **2017**, *56*, 6803−6807.
(17) Wang, M.; Wu, X.-P.; Zheng, S.; Zhao, L.; Li, L.; Shen, L.; Gao, Y.; Xue, N.; Guo, X.; Huang, W.; Gan, Z.; Blanc, F.; Yu, Z.; Ke, X.; Ding, W.; Gong, X.-Q.; Grey, C. P.; Peng, L. Identification of

Different Oxygen Species in Oxide Nanostructures with ^{17}O Solid-State NMR Spectroscopy. *Sci. Adv.* **2015**, *1*, No. e1400133.
(18) Chen, J.; Wu, X.-P.; Hope, M. A.; Qian, K.; Halat, D. M.; Liu, T.; Li, Y.; Shen, L.; Ke, X.; Wen, Y.; Du, J.-H.; Magusin, P. C. M. M.; Paul, S.; Ding, W.; Gong, X.-Q.; Grey, C. P.; Peng, L. Polar Surface Structure of Oxide Nanocrystals Revealed with Solid-State NMR Spectroscopy. *Nat. Commun.* **2019**, *10*, 5420.
(19) Chen, J.; Hope, M. A.; Lin, Z.; Wang, M.; Liu, T.; Halat, D. M.; Wen, Y.; Chen, T.; Ke, X.; Magusin, P. C. M. M.; Ding, W.; Xia, X.; Wu, X.-P.; Gong, X.-Q.; Grey, C. P.; Peng, L. Interactions of Oxide Surfaces with Water Revealed with Solid-State NMR Spectroscopy. *J. Am. Chem. Soc.* **2020**, *142*, 11173−11182.
(20) Chen, J.; Wu, X.-P.; Hope, M. A.; Lin, Z.; Zhu, L.; Wen, Y.; Zhang, Y.; Qin, T.; Wang, J.; Liu, T.; Xia, X.; Wu, D.; Gong, X.-Q.; Tang, W.; Ding, W.; Liu, X.; Chen, L.; Grey, C. P.; Peng, L. Surface Differences of Oxide Nanocrystals Determined by Geometry and Exogenously Coordinated Water Molecules. *Chem. Sci.* **2022**, *13*, 11083−11090.
(21) Li, Y.; Wu, X.-P.; Jiang, N.; Lin, M.; Shen, L.; Sun, H.; Wang, Y.; Wang, M.; Ke, X.; Yu, Z.; Gao, F.; Dong, L.; Guo, X.; Hou, W.; Ding, W.; Gong, X.-Q.; Grey, C. P.; Peng, L. Distinguishing Faceted Oxide Nanocrystals with ^{17}O Solid-State NMR Spectroscopy. *Nat. Commun.* **2017**, *8*, 581.
(22) Champouret, Y.; Coppel, Y.; Kahn, M. L. Evidence for Core Oxygen Dynamics and Exchange in Metal Oxide Nanocrystals from In Situ ^{17}O MAS NMR. *J. Am. Chem. Soc.* **2016**, *138*, 16322−16328.
(23) Song, B.; Li, Y.; Wu, X.-P.; Wang, F.; Lin, M.; Sun, Y.; Jia, A.-p.; Ning, X.; Jin, L.; Ke, X.; Yu, Z.; Yang, G.; Hou, W.; Ding, W.; Gong, X.-Q.; Peng, L. Unveiling the Surface Structure of ZnO Nanorods and H_2 Activation Mechanisms with ^{17}O NMR Spectroscopy. *J. Am. Chem. Soc.* **2022**, *144*, 23340−23351.
(24) Du, J.-H.; Chen, L.; Zhang, B.; Chen, K.; Wang, M.; Wang, Y.; Hung, I.; Gan, Z.; Wu, X.-P.; Gong, X.-Q.; Peng, L. Identification of CO_2 adsorption sites on MgO nanosheets by solid-state nuclear magnetic resonance spectroscopy. *Nat. Commun.* **2022**, *13*, 707.
(25) Yang, C.; Wang, J.; Xia, X.; Ding, L.; Wen, Y.; Zhao, T.; Ke, X.; Gong, X.-Q.; Wu, X.-P.; Ding, W.; Peng, L. Can Subsurface Oxygen Species in Oxides Participate in Catalytic Reactions? An ^{17}O Solid-State Nuclear Magnetic Resonance Study. *J. Phys. Chem. Lett.* **2024**, *15*, 8218−8223.
(26) Wen, Y.; Zhang, W.; Wen, J.; Wang, F.; Ke, X.; Chen, J.; Peng, L. Tracking the Facet Transformation of CeO_2 by ^{17}O Solid-State Nuclear Magnetic Resonance. *J. Phys. Chem. Lett.* **2024**, *15*, 11587−11592.
(27) Du, J.-H.; Peng, L. Recent Progress in Investigations of Surface Structure and Properties of Solid Oxide Materials with Nuclear Magnetic Resonance Spectroscopy. *Chin. Chem. Lett.* **2018**, *29*, 747−751.
(28) George, S. M. Atomic Layer Deposition: An Overview. *Chem. Rev.* **2010**, *110*, 111−131.
(29) Justin Kunene, T.; Kwanda Tartibu, L.; Ukoba, K.; Jen, T.-C. Review of Atomic Layer Deposition Process, Application and Modeling Tools. *Mater. Today* **2022**, *62*, S95−S109.
(30) Cremers, V.; Puurunen, R. L.; Dendooven, J. Conformality in Atomic Layer Deposition: Current Status Overview of Analysis and Modelling. *Appl. Phys. Rev.* **2019**, *6*, No. 021302.
(31) Lu, J.; Fu, B.; Kung, M. C.; Xiao, G.; Elam, J. W.; Kung, H. H.; Stair, P. C. Coking- and Sintering-Resistant Palladium Catalysts Achieved Through Atomic Layer Deposition. *Science* **2012**, *335*, 1205−1208.
(32) Burton, B. B.; Goldstein, D. N.; George, S. M. Atomic Layer Deposition of MgO Using Bis(ethylcyclopentadienyl)magnesium and H_2O. *J. Phys. Chem. C* **2009**, *113*, 1939−1946.
(33) Tynell, T.; Karppinen, M. Atomic Layer Deposition of ZnO: A Review. *Semicond. Sci. Technol.* **2014**, *29*, No. 043001.
(34) Blanquart, T.; Niinistö, J.; Ritala, M.; Leskelä, M. Atomic Layer Deposition of Groups 4 and 5 Transition Metal Oxide Thin Films: Focus on Heteroleptic. *Chem. Vap. Deposition* **2014**, *20*, 189−208.
(35) Kwak, J. H.; Hu, J.; Mei, D.; Yi, C.-W.; Kim, D. H.; Peden, C. H. F.; Allard, L. F.; Szanyi, J. Coordinatively Unsaturated Al^{3+} Centers as Binding Sites for Active Catalyst Phases of Platinum on γ-Al_2O_3. *Science* **2009**, *325*, 1670−1673.
(36) Trueba, M.; Trasatti, S. P. γ-Alumina as a Support for Catalysts: A Review of Fundamental Aspects. *Eur. J. Inorg. Chem.* **2005**, *2005*, 3393−3403.
(37) Prins, R. On the structure of γ-Al_2O_3. *J. Catal.* **2020**, *392*, 336−346.
(38) Kentgens, A. P. M. A Practical Guide to Solid-State NMR of Half-Integer Quadrupolar Nuclei with Some Applications to Disordered Systems. *Geoderma* **1997**, *80*, 271−306.
(39) Shen, L.; Wang, Y.; Du, J.-H.; Chen, K.; Lin, Z.; Wen, Y.; Hung, I.; Gan, Z.; Peng, L. Probing Interactions of γ-Alumina with Water via Multinuclear Solid-State NMR Spectroscopy. *ChemCatChem* **2020**, *12*, 1569−1574.
(40) Medek, A.; Harwood, J. S.; Frydman, L. Multiple-Quantum Magic-Angle Spinning NMR: A New Method for the Study of Quadrupolar Nuclei in Solids. *J. Am. Chem. Soc.* **1995**, *117*, 12779−12787.
(41) Engelhardt, G.; Kentgens, A. P. M.; Koller, H.; Samoson, A. Strategies for Extracting NMR Parameters from ^{23}Na MAS, DOR and MQMAS spectra. A Case Study for $Na_4P_2O_7$. *Solid State Nucl. Magn. Reson.* **1999**, *15*, 171−180.
(42) Wang, Q.; Li, W.; Hung, I.; Mentink-Vigier, F.; Wang, X.; Qi, G.; Wang, X.; Gan, Z.; Xu, J.; Deng, F. Mapping the Oxygen Structure of γ-Al_2O_3 by High-Field Solid-State NMR Spectroscopy. *Nat. Commun.* **2020**, *11*, 3620.
(43) Li, W.; Wang, Q.; Xu, J.; Aussenac, F.; Qi, G.; Zhao, X.; Gao, P.; Wang, C.; Deng, F. Probing the Surface of γ-Al_2O_3 by Oxygen-17 Dynamic Nuclear Polarization Enhanced Solid-State NMR Spectroscopy. *Phys. Chem. Chem. Phys.* **2018**, *20*, 17218−17225.
(44) Yang, S.; Park, K. D.; Oldfield, E. Oxygen-17 Labeling of Oxides and Zeolites. *J. Am. Chem. Soc.* **1989**, *111*, 7278−7279.
(45) Kovarik, L.; Genc, A.; Wang, C.; Qiu, A.; Peden, C. H. F.; Szanyi, J.; Kwak, J. H. Tomography and High-Resolution Electron Microscopy Study of Surfaces and Porosity in a Plate-like γ-Al_2O_3. *J. Phys. Chem. C* **2013**, *117*, 179−186.
(46) Chen, K.; Zornes, A.; Nguyen, V.; Wang, B.; Gan, Z.; Crossley, S. P.; White, J. L. ^{17}O Labeling Reveals Paired Active Sites in Zeolite Catalysts. *J. Am. Chem. Soc.* **2022**, *144*, 16916−16929.
(47) Wischert, R.; Copéret, C.; Delbecq, F.; Sautet, P. Optimal Water Coverage on Alumina: A Key to Generate Lewis Acid−Base Pairs that are Reactive Towards the C-H Bond Activation of Methane. *Angew. Chem., Int. Ed.* **2011**, *50*, 3202−3205.
(48) Wischert, R.; Florian, P.; Copéret, C.; Massiot, D.; Sautet, P. Visibility of Al Surface Sites of γ-Alumina: A Combined Computational and Experimental Point of View. *J. Phys. Chem. C* **2014**, *118*, 15292−15299.
(49) Wischert, R.; Laurent, P.; Copéret, C.; Delbecq, F.; Sautet, P. γ-Alumina: The Essential and Unexpected Role of Water for the Structure, Stability, and Reactivity of "Defect" Sites. *J. Am. Chem. Soc.* **2012**, *134*, 14430−14449.
(50) Duan, H.; You, R.; Xu, S.; Li, Z.; Qian, K.; Cao, T.; Huang, W.; Bao, X. Pentacoordinated Al^{3+}-Stabilized Active Pd Structures on Al_2O_3-Coated Palladium Catalysts for Methane Combustion. *Angew. Chem., Int. Ed.* **2019**, *58*, 12043−12048.

https://doi.org/10.1021/acs.jpclett.5c01138
J. Phys. Chem. Lett. 2025, 16, 6907−6913